PHYSICS OF FLUIDS VOLUME 13, NUMBER 11 NOVEMBER 2001

Experimental study of the mixing transition in a gaseous axisymmetric jet

T. R. Meyer and J. C. Dutton
Department of Mechanical and Industrial Engineering, University of Illinois at Urbana-Champaign, Urbana, Illinois 61801

R. P. Lucht
Department of Mechanical Engineering, Texas A&M University, College Station, Texas 77843

(Received 4 May 2001; accepted 2 August 2001)

Instantaneous, quantitative, planar images of molecularly mixed-jet fluid fraction were obtained for the purpose of studying the mixing transition in a gaseous axisymmetric jet from $\mathrm{Re}_D = 16\,200–29\,200$. By using a simultaneous nitric oxide and acetone planar laser-induced fluorescence technique, the mixing transition was detected from sudden changes in the molecularly mixed-jet fluid volume fraction, the growth rate of the shear layer, the preferred mixed-jet fluid fraction, and the character of axial/radial probability density functions. The mixing transition for all Reynolds numbers in this regime was found to begin after the first vortex pairing near $Rx/\lambda = 6$ and was completed by the second vortex pairing near $Rx/\lambda = 12$, where $R = (1-r)/(1+r)$, r is the low-to high-speed freestream velocity ratio, and λ is the natural instability wavelength. The statistical quantities at all Reynolds numbers were found to collapse when scaled with Rx/λ, with the exception of the mixing layer width. The latter collapsed for all Reynolds numbers when scaled by Rx/λ prior to the mixing transition, and by x/D beyond the mixing transition, as expected for turbulent jets for which $r \approx 0$. [DOI: 10.1063/1.1405441]

I. INTRODUCTION

Two-dimensional planar and axisymmetric mixing layers are fundamental flowfields that have been used extensively for the study of turbulent scalar transport and mixing. The mixing transition is perhaps the most dominant aspect of near-field mixing layer dynamics, and is associated with the breakdown of the diffusion layers within the large-scale Kelvin–Helmholtz rollers into small-scale eddies. Such small-scale motions increase the local interfacial area between the pure fluid streams, and result in a sudden and dramatic increase in mixing.[1] Understanding the dynamics of entrainment and mixing in the near-field region of such mixing layers is important for many chemical processing and combustion applications for which the asymptotic, self-similar state in the far-field region is not typically attained.

The goal of this investigation is to study the location and nature of the mixing transition in the near field of an initially laminar gaseous jet, as well as to characterize the composition of the shear layer prior to, during, and beyond the transition. This is accomplished using a recently developed combined passive-scalar and cold-chemistry planar laser-induced fluorescence (PLIF) technique for instantaneous, planar imaging of molecularly mixed fluid quantities. King *et al.*[2,3] first applied this technique in the near field of gaseous jets for a variety of Reynolds numbers between $\mathrm{Re}_D = 1000–100\,000$. The jet at $\mathrm{Re}_D = 10\,000$ did not undergo a mixing transition, while their next measurement at $\mathrm{Re}_D = 30\,000$ was already beyond the early stages of transition. The current investigation will focus on Reynolds numbers from $\mathrm{Re}_D = 16\,200–29\,200$, since it is within this range that King *et al.*[2,3] reported a marked change in the mixed-jet fluid fraction statistics, and is the range most conducive to studying the mixing transition. Quantitative imaging of gaseous shear layer molecular mixing (instantaneous or time-averaged) has not, to our knowledge, been performed in this regime.

II. BACKGROUND

Early flow visualization work has shown that mixing in the near field (close to the splitter plate or nozzle lip) is dominated by large-scale Kelvin–Helmholtz roller structures that entrain pure fluid from either stream across the entire width of the mixing layer.[4,5] Subsequent hot-wire experiments in plane mixing layers have shown that small-scale eddies begin to appear only after these vortex structures merge and interact with streamwise vortices.[6,7] A direct numerical simulation of the mixing transition in a time-developing plane mixing layer further indicated that the streamwise vortices in the braid regions of adjacent Kelvin–Helmholtz rollers are engulfed as the rollers pair.[8] The interaction of the high-vorticity regions within these roller structures also contributes to the breakdown to small-scale eddies. At lower Reynolds numbers, for which streamwise vortices in the braid regions are not supported, vortex core fluctuations and oblique instability modes have been suggested as alternative mechanisms for small-scale transition during a vortex pairing.[9] The common element in these studies is that the breakdown to small-scale turbulence requires the interaction of three-dimensional instabilities with the pairing of Kelvin–Helmholtz roller structures.

This analysis can also be applied to high-Reynolds number axisymmetric mixing layers, which are thin compared to the nozzle diameter and can support Kelvin–Helmholtz rollers, streamwise vortices, oblique modes, as well as azimuthal instabilities.[10,11] The azimuthal mode has been cited as a possible cause for increased mixing exhibited by axisymmetric shear layers,[12] and will be of further interest in the discussion of the current experimental results. Indeed, recent studies at high-Reynolds numbers ($Re_D \geqslant 30\,000$) have confirmed that the appearance of small-scale turbulence in gaseous jets takes place quite early in the developing shear layer and prior to the end of the jet potential core.[13,14] The importance of three-dimensional instabilities in the small-scale transition of gaseous jets is further supported by experiments at low jet Reynolds numbers ($Re_D \leqslant 10\,000$) that failed to produce a detectable mixing transition.[13,15]

The occurrence of vortex pairing in conjunction with the creation of small-scale eddies suggests that for Reynolds numbers above a certain threshold value ($Re_D > 10\,000$ for axisymmetric jets), the mixing transition can be predicted from the initial two-dimensional instability wavelength. Huang and Ho[7] suggested that an appropriate length scale for the merging of coherent structures, and thus the location of the mixing transition, should account for the initial instability wavelength, λ, as well as the velocity ratio, r. In this case, r is defined as the velocity ratio of the low- to high-speed fluid streams. They further used the parameter $R=(1-r)/(1+r)$, which accounts for the ratio between the rates of deformation (velocity difference) and advection (average velocity). Scaling the axial coordinate as Rx/λ, Huang and Ho[7] found that the first vortex merging under a variety of conditions in a gaseous planar shear layer occurs at $Rx/\lambda \approx 4$, and that the second merging occurs at $Rx/\lambda \approx 8$. They also found that random fine eddies, perhaps indicative of a small-scale transition, are first detected in the core regions of vortices during the first pairing event near $Rx/\lambda \approx 4$. Ho and Huerre[16] plotted the roll-off exponent of the velocity spectra from a number of investigations and found that it reached the asymptotic turbulent value of $-5/3$ by $Rx/\lambda \approx 8$, or about the second pairing. In a more direct measure of scalar mixing, Breidenthal[17] found that the amount of product in a reacting shear layer increases dramatically from $Rx/\lambda \approx 8-12$, indicating that the scalar field may develop more slowly than the velocity field. It should be kept in mind, therefore, that the *mixing transition* is not necessarily synonymous with what is typically referred to as the *turbulent transition*, though both involve a cascade from large to small scales.

There is also growing evidence that the composition of the scalar field beyond the mixing transition undergoes a slow evolution in the radial distribution of the statistically preferred mixture fraction.[13,18–20] Karasso and Mungal[18] reviewed a number of previous studies of the scalar field in planar liquid and gaseous shear layers and found that the character of the mixed fluid probability density functions (PDFs) plotted across the shear layer typically undergoes a change from stationary to marching/tilted at $Rx/\lambda \approx 22$. This is well beyond the mixing transition and well beyond the hydrodynamic fully developed condition expected at $Rx/\lambda \approx 16$.

King *et al.*[13] found that a similar evolution occurs in the scalar-field statistics of gaseous axisymmetric jets. They did not study the mixing transition, but they concluded that an evolution from stationary to marching/tilted PDFs occurs at $Rx/\lambda \approx 12-14$, which is much earlier than the value of $Rx/\lambda \approx 22$ from the planar shear layers described above. This suggests that the dynamics of axisymmetric and planar shear layers are somewhat different, and that the pairing parameter alone cannot predict universal characteristics of the mixing field. Thus, it will be of interest in this investigation to determine if the pairing parameter can be used to predict the mixing transition for jets with different Reynolds numbers within the same axisymmetric flow regime studied by King *et al.*,[13] as well as to consider possible differences between planar and axisymmetric shear layer mixing.

III. EXPERIMENTAL APPROACH

A number of techniques have been used to study the scalar field in axisymmetric and planar shear layers. They typically fall into two categories, which can be referred to as passive scalar and chemically reactive. In the passive-scalar technique, a tracer molecule is seeded into one of the fluid streams, and the fluid concentration in the mixing layer can be determined by the drop in signal relative to the signal from the seeded freestream. It is well known that passive-scalar techniques over-predict the extent of molecular mixing, however, since the fluid from a probe volume of a size that exceeds the smallest diffusion length scales may not be mixed at the molecular level.[13,18]

Chemically reactive techniques have the advantage that the measured signal is sensitive to the state of molecular mixing. This provides a resolution-independent measure of the probe-volume averaged molecularly mixed fluid fraction. Note that both passive-scalar and chemically reactive techniques are probe-volume averaged, but unlike chemically reactive techniques, passive-scalar techniques cannot distinguish between mixed and unmixed fluid within the probe volume. In the case of PLIF of acid-base reactions, for example, the measured chemical product is used to indicate the amount of molecularly mixed fluid in the probe volume.[17,18,21] Unfortunately, this technique is only applicable in liquid flows. Cold-wire thermometry of low-heat release reactions is based on a similar premise, but the amount of molecularly mixed fluid in this case is proportional to the measured temperature.[22,23] This method relies on physical point probes, however, and has considerable disadvantages in spatial and temporal resolution when compared with laser imaging techniques. Planar laser Mie scattering has been used in supersonic gaseous flows, for which the extent of molecular mixing is marked by the amount of seeded low-speed fluid that has condensed due to contact with the colder high-speed stream.[12] This method is only qualitative, however, in that the measured signal is affected by the locally varying thermodynamic state of the mixing layer. In the case of cold-chemistry nitric oxide (NO) PLIF, the imaged fluorescence signal indicates the amount of molecularly *unmixed* fluid because NO fluorescence is almost entirely quenched when it is molecularly mixed with oxygen from the co-flowing stream.[12] Thus, ''flip'' experiments are required to obtain the *time-averaged* probability of molecularly mixed fluid. The obvious disadvantage of this technique

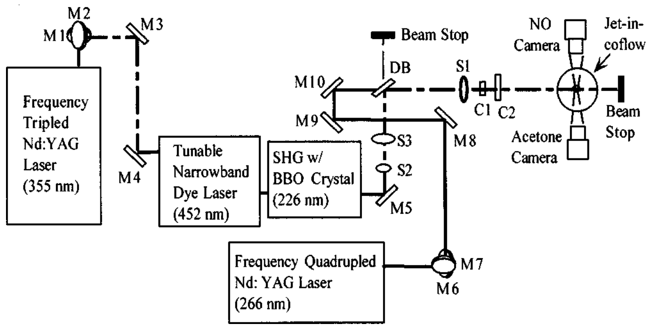

FIG. 1. Dual-tracer PLIF lasers and optics. $M1-M4$:355 nm mirrors. $M5$:226 nm mirror. $M6-10$:266 nm mirrors. $S1$:$f=1$ m spherical lens. $S2$:$f=-50$ mm spherical lens. $S3$:$f=100$ mm spherical lens. $C1$:$f=-19$ mm cylindrical lens. $C2$:$f=150$ mm cylindrical lens. DB: dichroic beamsplitter.

is that it is incapable of measuring the instantaneous molecularly mixed fluid structure.

The dual-tracer PLIF technique used in the current investigation uses simultaneous passive-scalar and cold-chemistry tracers to mark the total and unmixed jet fluid. The difference of these two quantities provides the amount of molecularly mixed jet fluid on an instantaneous, planar basis. This technique has been described extensively in previous investigations,[2,13] and is summarized below.

The jet fluid is N_2 seeded with NO, and the co-flow is air seeded with acetone. As shown in Fig. 1, the technique requires coincident laser sheets at 226 and 266 nm for NO and acetone PLIF, respectively. These sheets are formed by the spherical ($S1$) and cylindrical lenses ($C1$ and $C2$) to a thickness of about 250 μm. Simultaneous images of NO and acetone PLIF are acquired using two 512×512 unintensified CCD cameras on opposite sides of the jet with imaged flow-field areas of 51 μm$\times$51 μm per pixel. Once acquired, the acetone images are remapped to the same scale and orientation as the NO images. After background subtraction and corrections for laser sheet intensity variations, the NO and acetone PLIF signals from the mixing layer are normalized by reference signals from the pure jet and co-flow regions, respectively. The typical signal-to-noise ratio (SNR) is 40:1 for both the NO and acetone PLIF.

As indicated by Eqs. (1) and (2) below, the NO PLIF signal, $S_{f,\mathrm{NO}}$, is used to obtain the fraction of pure jet fluid, f_{pjet}, while the acetone PLIF signal, $S_{f,\mathrm{ac}}$, is used to obtain the fraction of total co-flow fluid, f_{tcf}. The fraction of molecularly mixed jet fluid, f_{mjet}, can be obtained from Eq. (3) as the difference between the fractions of total jet and pure jet fluids. A mixing efficiency, η_{mjet}, is also defined by Eq. (4) as the ratio of mixed jet to total jet fluid. Since Eq. (1) is only valid assuming an infinite quenching rate of NO PLIF in the presence of oxygen and acetone, however, a correction for finite quenching using a two-level model is incorporated into the image processing procedure.[13,15] We emphasize that these quantities are obtained on a pixel-by-pixel basis in each instantaneous image.

$$f_{\mathrm{pjet}}=\frac{S_{f,\mathrm{NO}}(\text{mixing layer})}{S_{f,\mathrm{NO}}(\text{pure jet})}, \tag{1}$$

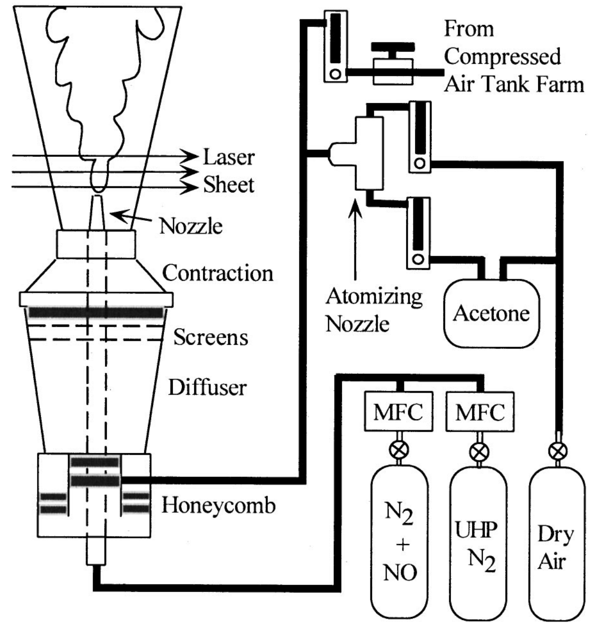

FIG. 2. Schematic of the jet-in-co-flow facility.

$$f_{\mathrm{tcf}}=\frac{S_{f,\mathrm{ac}}(\text{mixing layer})}{S_{f,\mathrm{ac}}(\text{pure co-flow})}=1-f_{\mathrm{tjet}}, \tag{2}$$

$$f_{\mathrm{mjet}}=f_{\mathrm{tjet}}-f_{\mathrm{pjet}}=1-f_{\mathrm{tcf}}-f_{\mathrm{pjet}}, \tag{3}$$

$$\eta_{\mathrm{mjet}}=\frac{f_{\mathrm{mjet}}}{f_{\mathrm{tjet}}}=\frac{1-f_{\mathrm{tcf}}-f_{\mathrm{pjet}}}{1-f_{\mathrm{tcf}}}. \tag{4}$$

The definition of mixed jet fluid volume fraction is shown in Eq. (5), and the probability density function of f_{mjet} is normalized to unity as shown in Eq. (6):

$$\frac{V_{\mathrm{mj}}}{V}=\frac{2\int_{r_i}^{r_o}\langle f_{\mathrm{mjet}}\rangle r\,dr}{(r_o^2-r_i^2)}, \tag{5}$$

$$\int_0^1 P(f_{\mathrm{mjet}},\xi)\,df_{\mathrm{mjet}}=1, \tag{6}$$

where r_i and r_o are the inner and outer radii of the mixing layer, respectively, $\langle f_{\mathrm{mjet}}\rangle$ is the ensemble-averaged mixed-jet fluid fraction, and ξ is r/D or x/D for radial or axial PDFs, respectively. Scalar dissipation, as defined in Eq. (7), is used in this investigation to detect high concentration gradients:

$$\text{Scalar Dissipation}=\nabla C\cdot\nabla C, \tag{7}$$

where ∇C for this case is the two-dimensional gradient of the concentration of total jet fluid calculated from second-order central differencing. The scalar dissipation beyond the mixing transition is only qualitative, however, due to the increased subresolution stirring and three-dimensionality in this regime.

The jet-in-co-flow facility is shown in Fig. 2. The jet fluid (N_2) is seeded at 300 ppm with NO and is fed into a 21.5 mm diameter vertical tube which tapers to a 5 mm nozzle-exit diameter. Co-flow air from a compressed air tank farm is seeded with acetone at 4.6% by mass and is passed

TABLE I. Flow conditions.

Re_D	16 200	22 700	29 200
U_1 (m/s)	47.4	66.5	85.5
$r = U_2/U_1$[a]	0.0057	0.0041	0.0032
$Re_\delta = \Delta U \delta_{5\%}/\nu$	3100–30 700	4500–42 600	7700–48 700
L_D (μm)[b]	34–64	26–50	21–41
f_0 (Hz)[c]	14 000	23 700	37 000
λ (mm)[d]	1.70	1.40	1.15
Rx/λ[e]	2.1–15	2.6–19	3.2–22
θ_i (mm)[f]	0.0414	0.0349	0.0313
St_θ[g]	0.0122	0.0124	0.0135
u_i'/U_1 (%)[h]	0.22	0.40	0.56

[a] U_1, U_2 = jet and co-flow fluid velocities, respectively.
[b] L_D = diffusion length scale = $11.2\delta\, Re_\delta^{-3/4}\, Sc^{-1/2}$ (Ref. 24).
[c] f_0 = fundamental axisymmetric instability frequency.
[d] λ = natural instability wavelength = $U_{ave}/2f_0$.
[e] $R = (1-r)/(1+r)$.
[f] θ_i = measured initial shear layer momentum thickness.
[g] St_θ = Strouhal number = $f_0\theta_i/U_1$.
[h] u_i'/U_1 = initial turbulence intensity.

through five honeycomb rings and two mesh screens before exiting through a 16 cm diameter opening. Tylan mass flow controllers with ± 0.2% full-scale repeatability and ± 1% full-scale accuracy were used to measure the average jet-exit and co-flow fluid velocities; spatial velocity profiles and turbulence statistics were obtained using hot-film anemometry.

IV. RESULTS AND DISCUSSION

A. Flow conditions

As shown in Table I, the flow conditions studied in the current investigation correspond to jet Reynolds numbers of $Re_D = 16\,200$, 22 700, and 29 200. The axial extent of all PLIF images ranged from $x/D = 1-5.25$, corresponding to Reynolds numbers of $Re_\delta = 3100-48\,700$ based on the local ± 5% mixing-layer width. The smallest diffusion length scale, estimated from the results of Buch and Dahm,[24] ranged from 21 to 64 μm. This is of the same order as the pixel resolution of 51 μm, but is significantly smaller than the laser-sheet width of about 250 μm.

Calculation of the pairing parameter, Rx/λ, required measurements of the fundamental axisymmetric instability mode, f_0, from hot-film velocity spectra within the shear layer. Appropriate care was taken to differentiate f_0 from the first helical mode, f_1, and several identifiable sub-harmonics.[25] As expected, the fundamental axisymmetric and helical modes differed in frequency by 17%–20%. Values of f_0 measured in this manner exhibited a strong linear dependence on $U_{ave}^{3/2}$ as expected for shear layers with low velocity ratios and with laminar initial conditions. The initial instability wavelength was then be found from $\lambda = U_{ave}/2f_0$, which represents the initial vortex spacing of the fundamental axisymmetric mode. The resulting values of Rx/λ, shown in Table I, range from 2.1 to 22. Since the value of $R = (1-r)/(1+r)$ is nearly unity for all jet Reynolds numbers in the current study, only x/λ is varied here. Nonetheless, the notation Rx/λ is used as a reminder that comparisons with other investigations should account for nonunity values of R.

The initial shear layer momentum thickness, θ_i, was obtained by extrapolating hot-film measurements near the nozzle lip $(0.07 < x/D < 0.23)$ to the nozzle exit plane. The momentum thickness grew linearly with axial distance in this region, and the extrapolated values of θ_i shown in Table I exhibit the expected linear dependence on $Re_D^{-1/2}$. The maximum initial-momentum-thickness to jet-diameter ratio is about 1:125. The shape factors at the nozzle exit plane (not listed in Table I) were also measured using hot-film anemometry, and differed from the Blasius profile by about 5% for all three Re_D. Excellent agreement was obtained between measured and hyperbolic-tangent cross-stream velocity profiles.

The Strouhal number, St_θ, is found from $f_0\theta_i/U_1$. According to linear stability theory, the most amplified axisymmetric mode, given an initially laminar shear layer and hyperbolic-tangent mean velocity profile, is $St_\theta = 0.017$.[26,27] Previous measurements in gaseous jets have found a range of St_θ from 0.009 to 0.018.[28] In the current study, $St_\theta = 0.0122$, 0.0124, and 0.0135 for $Re_D = 16\,200$, 22 700, and 29 200, respectively. This is the range found by Husain and Hussain to represent the natural instability frequency,[29] or the frequency that is most receptive to feedback from downstream pairing events. Thus, the value of $\lambda = U_{ave}/2f_0$ in the current investigation may differ from other investigations that assume a value of $St_\theta = 0.017$.

In addition to average velocity data and velocity spectra, measurements of the peak turbulence intensity, u'/U_1, were made at various axial locations. As listed in Table I, the turbulence intensity at the exit plane is 0.22%, 0.40%, and 0.56% for $Re_D = 16\,200$, 22 700, and 29 200, respectively. The values of peak u'/U_1 increase very slowly in the laminar nozzle-exit region for all three Reynolds numbers, then undergo a sudden increase at about $Rx/\lambda = 2.5$ (near the location vortex roll-up). The values of peak u'/U_1 have maxima near $Rx/\lambda = 9$ and, in agreement with results from previous investigations,[16] reach an asymptotic state between $Rx/\lambda = 10-12$. As will be shown later in the discussion of mixed-fluid probability density functions, the range of $Rx/\lambda = 10-12$ corresponds to the final stages of the mixing transition.

B. Instantaneous images

Typical instantaneous images of the mixed-jet fluid fraction, f_{mjet}, are shown in Fig. 3 for $Re_D = 16\,200$ and $Re_D = 22\,700$. It is immediately apparent from these images that the Kelvin–Helmholtz rollers and large-scale structures further downstream are asymmetric for both Reynolds numbers, and that the instantaneous near- and far-field structure vary significantly from shot-to-shot. Thus, a transition to smaller scales is quite evident in all the images, but it is difficult to define its precise location. Foregoing an exact definition for the moment, a number of qualitative trends can be identified to help characterize the location and nature of the transition: (1) The size and spacing of the vortices decrease as Reynolds number increases; (2) the transition to smaller scales occurs

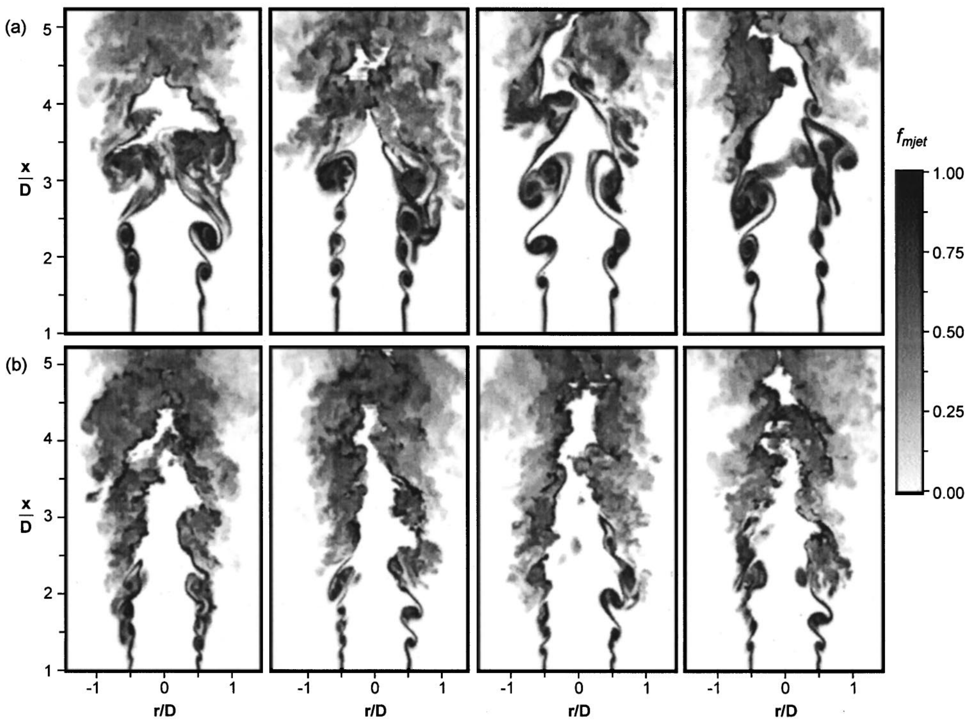

FIG. 3. Instantaneous images of mixed jet fluid fraction, f_{mjet}, at (a) $\mathrm{Re}_D = 16\,200$ and (b) $\mathrm{Re}_D = 22\,700$.

further upstream as Reynolds number increases; and (3) vortex pre-pairing events can be seen in nearly all the images prior to the small-scale transition. This supports the use of an axial scaling based on the pairing parameter, Rx/λ, which accounts for the initial instability wavelength of the shear layer. As mentioned previously, Huang and Ho[7] found that the first vortex pairing event in a planar shear layer typically takes place at $Rx/\lambda = 4$. Based on the velocity ratios and initial instability wavelengths shown in Table I, $Rx/\lambda = 4$ corresponds to $x/D = 1.36$, 1.12, and 0.92 for $\mathrm{Re}_D = 16\,200$, 22 700, and 29 200, respectively. These locations for vortex pairing are clearly not supported by the images in Fig. 3 ($\mathrm{Re}_D = 29\,200$ not shown), for which the initial vortex roll-up does not occur until $x/D > 1$. In fact, the average location of the first vortex pairing from the full set of instantaneous images was found to take place much further downstream at about $x/D = 2.00$, 1.63, and 1.25 for $\mathrm{Re}_D = 16\,200$, 22 700, and 29 200, respectively. It is unlikely that such a large discrepancy (~30%–50%) in the expected location of pairing between this work and that of Huang and Ho[7] could be due entirely to errors in measuring the velocity ratio and initial instability wavelength. The initial instability wavelength and average location of pairing measured at $\mathrm{Re}_D = 29\,200$ in the current investigation, for example, are in agreement with the measurements of King *et al.*[13] at $\mathrm{Re}_D = 30\,000$ ($\lambda/D \approx 0.17$, $x/D \approx 1.2$). It is highly likely, therefore, that the current data at $\mathrm{Re}_D = 29\,200$ and that of King *et al.*[13] at $\mathrm{Re}_D = 30\,000$ were, in fact, obtained at the same (though possibly both incorrectly measured) jet exit velocity conditions. Furthermore, King *et al.*[13] measured the same jet exit velocity as that measured in the current investigation (to within 3%) while using a completely different technique (from the pressure drop rather than the mass flow rate), implying that jet exit velocity and velocity ratio were measured correctly and consistently in both investigations.

Although it is difficult to make universal conclusions about the location of vortex pairing for all shear layers, it is significant that vortex pairing in the current investigation was found to occur fairly consistently at average Rx/λ values of 5.8, 5.8, and 5.4 for $\mathrm{Re}_D = 16\,200$, 22 700, and 29 200, respectively. These values are at larger multiples of the initial instability wavelength when compared with the planar shear layer of Huang and Ho.[7] In addition to different initial conditions, this discrepancy may result from the finite momentum thickness to jet diameter ratio ($\theta/D = 0.2 - 0.3$) near the location of the first vortex pairing for the current investigation.

The increase in the development time for pre-pairing vortices in this regime may increase the distortion of vortex rollers prior to pairing, enhance the peak negative vorticity in the core regions, and lead to a higher likelihood of small-scale transition after only the first pairing. Moser and Rogers[8] report, for example, that the peak negative spanwise vorticity for pre-pairing vortices in the transitional regime can be over six times the initial peak negative vorticity due to the distortion of vortex rollers. The agreement of the Rx/λ values for the first pairing at the different Reynolds numbers examined here further indicates that a common nondimensional location of the mixing transition may exist for these conditions. This can be confirmed by studying the mixed jet fluid statistics, but the current discussion is focused on the instantaneous composition in the evolution of the shear layer, as this will help in the physical interpretation of those statistics.

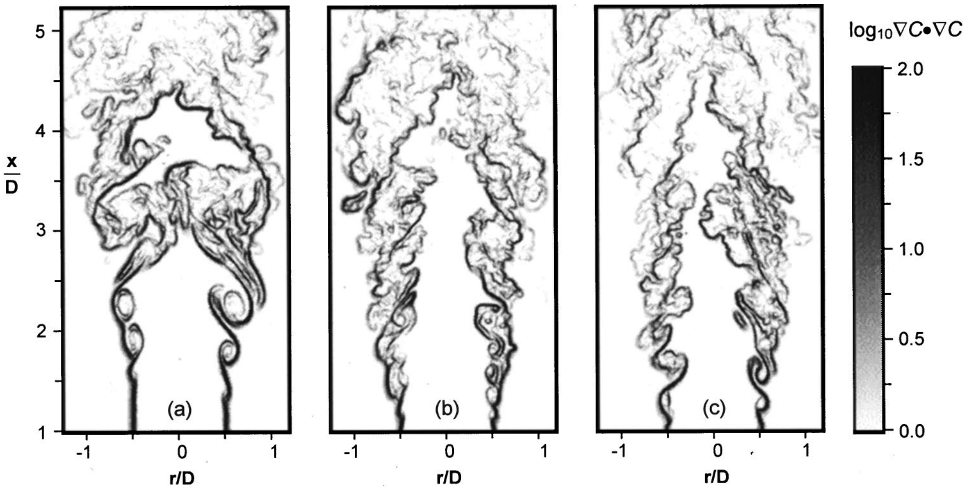

FIG. 4. Instantaneous images of two-dimensional scalar dissipation, $\nabla C \cdot \nabla C$, for (a) $Re_D=16\,200$, (b) $Re_D=22\,700$, and (c) $Re_D=29\,200$.

Instantaneous images of scalar dissipation, which highlight the diffusion layers between structures of varying composition, are shown in Fig. 4 for $Re_D=16\,200$, 22 700, and 29 200. Early in the development of the shear layer, high values of scalar dissipation are seen on both the jet and co-flow boundaries for all three Reynolds numbers. There is an intermediate axial range in which the organized structures become more convoluted, with complex interior diffusion layers [e.g., Fig. 4(a), $x/D\approx 3$]. The direct numerical simulations (DNS) results of Moser and Rogers[8] show that these may represent the remnants of high vorticity regions in the Kelvin–Helmholtz roller structures, along with rib vortices that were present in the braid region. These authors also found that thin sheets of spanwise vorticity within these structures undergo subsequent roll-ups that enhance the cascade to smaller scales. On the co-flow side of the convoluted layers, shown in Fig. 4, secondary structures with lower dissipation contour outlines begin to appear [e.g., Fig. 4(c), $x/D\approx 3$]. These secondary structure grow in prominence further downstream, but are almost entirely confined to the co-flow boundary region of the shear layer. Figure 4 also indicates that large-scale (primary) structures persist along almost the entire axial length of the jet boundary region for $Re_D=22\,700$ and 29 200 [Figs. 4(b) and 4(c)]. The apparent braid regions between these structures provide a mechanism for continued jet fluid entrainment into the shear layer. The high scalar-dissipation contour outlines around the entire periphery of these structures indicate that their interior composition may be fairly homogeneous.

While the plots of scalar dissipation in Fig. 4 can show the outlines of large- to mid-sized eddies, the current imaging resolution is incapable of resolving the smallest diffusion length scales (L_D in Table I). It is useful, therefore, to study the appearance of subresolution stirring of pure jet fluid from instantaneous maps of jet fluid mixing efficiency, η_{mjet}, which gives the ratio of molecularly mixed jet fluid to total jet fluid in a probe volume [see Eq. (4)]. Thus, regions of $\eta_{\mathrm{mjet}}=0$ are composed entirely of pure jet or co-flow fluid, and regions of $\eta_{\mathrm{mjet}}=1$ contain no pure jet fluid. Regions in which $0<\eta_{\mathrm{mjet}}<1$, on the other hand, indicate the presence of pure jet fluid parcels stirred on a subresolution scale with co-flow fluid or molecularly mixed jet fluid.

Maps of η_{mjet} for $Re_D=16\,200$, 22 700, and 29 200 are shown in Fig. 5, and indicate that the mixing layers at all three Reynolds numbers are primarily in the pure (η_{mjet}

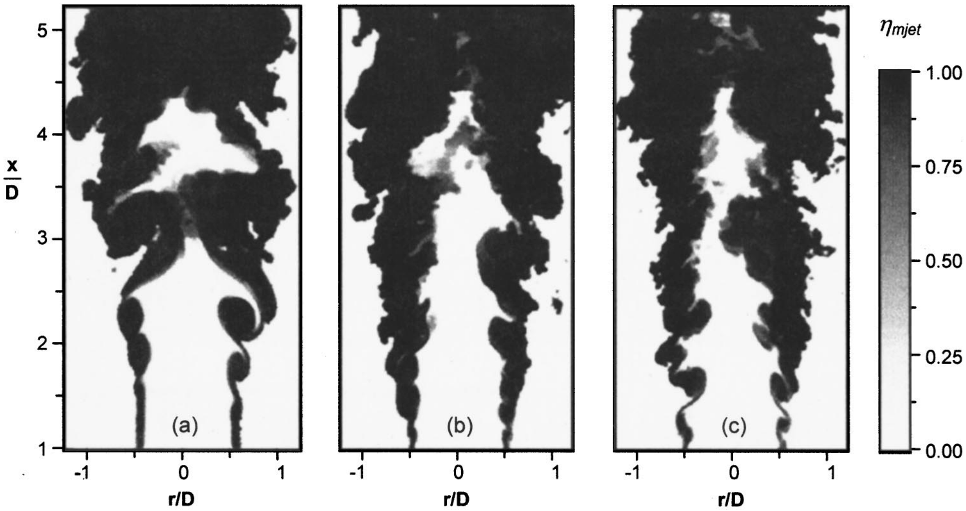

FIG. 5. Instantaneous images of jet fluid mixing efficiency, η_{mjet}, for (a) $Re_D=16\,200$, (b) $Re_D=22\,700$, and (c) $Re_D=29\,200$.

$=0$) or molecularly mixed ($\eta_{\text{mjet}}=1$) states. There are increased occurrences of partially mixed regions ($0<\eta_{\text{mjet}}<1$), however, at downstream locations on the jet side of the shear layer at all three Reynolds numbers. In addition, entrainment of pure jet fluid takes place in the braid regions of the primary structures identified in Fig. 4, and appear in Fig. 5 as intrusions of subresolution-stirred fluid [see Fig. 5(b), $x/D\approx 3$]. Note that these intrusions do not reach across the full width of the shear layer.

The fact that subresolution stirring of pure jet fluid is seen primarily on the jet interface does not preclude the existence of fine mixing scales in the middle and outer regions of the mixing layer since, by definition, maps of η_{mjet} can only indicate regions of pure jet fluid subresolution stirring. In the central region of the mixing layer, for example, a measurement volume may contain a fluid parcel with 80% mixed jet fluid that is being stirred with another fluid parcel at 20% mixed jet fluid, resulting in $\eta_{\text{mjet}}=1$. In addition, subresolution stirring may be present between molecularly mixed jet fluid and pure co-flow fluid on the outer edge of the mixing layer. Thus, the detection of pure jet fluid parcels on the jet interface of the mixing layer that are smaller than the limiting resolution of the imaging system ($\sim$250 μm) serves only as a positive indication that small mixing scales are present.

Of final interest from the instantaneous images is the mixed-jet fluid fraction itself, which was shown previously in Fig. 3, but is more easily studied on a quantitative basis using line plots. Figures 6 and 7 show radial line plots of mixed-jet fluid fraction for $\text{Re}_D=16\,200$ and $29\,200$, respectively, at various stages of mixing layer evolution. Also shown are the corresponding line plots of jet fluid mixing efficiency and the Rx/λ scaling of the axial coordinate [see right axes of Figs. 6(a) and 7(a)]. The mixed-jet fluid fraction in the near-exit vortex rollers of Row *A* remains near $f_{\text{mjet}}\approx 0.8$, with the exception of co-flow entrainment regions, for which the mixed-jet fluid fraction is expectedly low. These high values of f_{mjet} are maintained, even in the intermediate regime of Row *B*. As the shear layer develops, however, the mixed-jet fluid fraction begins to drop, and there appears to be a multilevel structure to the shear layer in Rows *C* and *D*, with a value of $f_{\text{mjet}}\approx 0.6$ near the jet core, a value of $f_{\text{mjet}}\approx 0.4$ in the center of the shear layer, and a value of $f_{\text{mjet}}\approx 0.2$ on the outermost edges. As is consistent with the existence of homogeneous large-scale structures, f_{mjet} remains fairly constant within each of these levels. While a variety of other profiles can be observed in the ensembles of instantaneous images, such as ramped values of f_{mjet}, the typical structure of f_{mjet} profiles has two or three fairly constant levels at these downstream locations. Remarkably similar multilevel mixing layer structures have also been found by Clemens and Mungal[20] to exist in compressible planar shear layers.

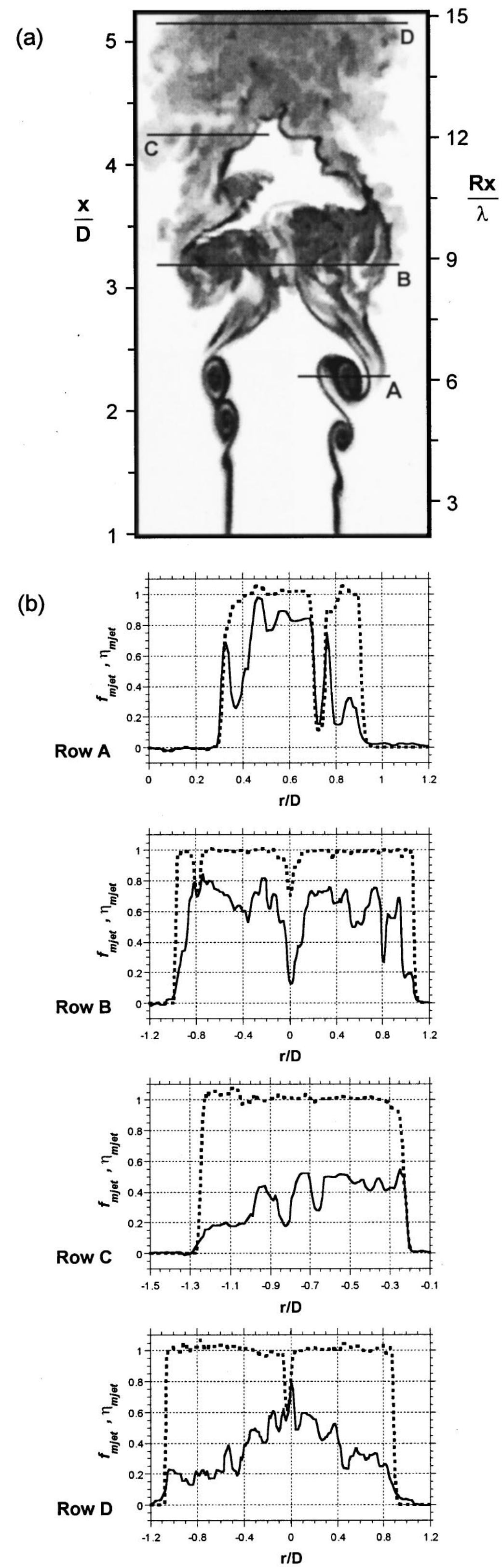

FIG. 6. (a) Instantaneous image of mixed jet fluid fraction, f_{mjet}, at $\text{Re}_D=16\,200$ and (b) line plots of f_{mjet} (——) and mixing efficiency, η_{mjet} (· · · ·).

C. Ensemble-averaged statistics

It seems clear from the instantaneous images that a *small-scale* transition occurs in the axisymmetric jet near field (prior to the end of the potential core) in the Reynolds number range of $\text{Re}_D=16\,200-29\,200$. This will be referred to hereafter as the *mixing* transition due to its dramatic impact on the composition of the shear layer, and on the nature of the entrainment and mixing processes. This section is fo-

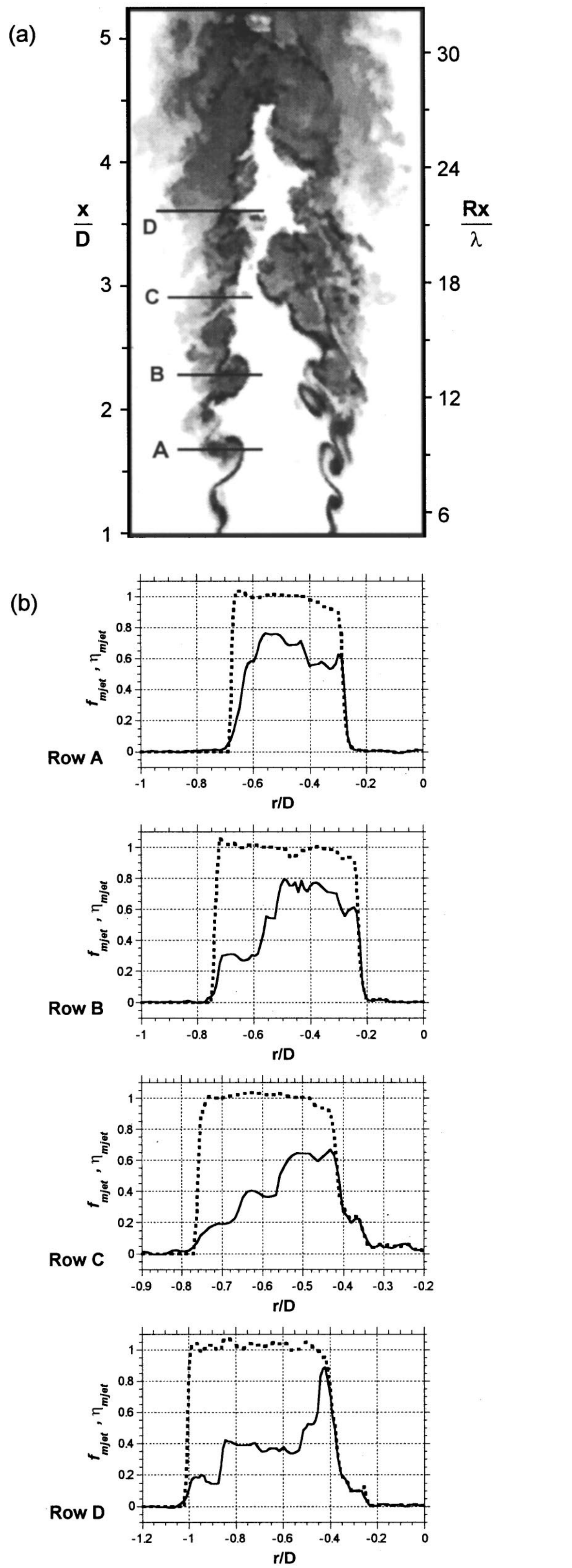

FIG. 7. (a) Instantaneous image of mixed jet fluid fraction, f_{mjet}, at $\mathrm{Re}_D = 29\,200$ and (b) line plots of f_{mjet} (——) and mixing efficiency, η_{mjet} (· · · ·).

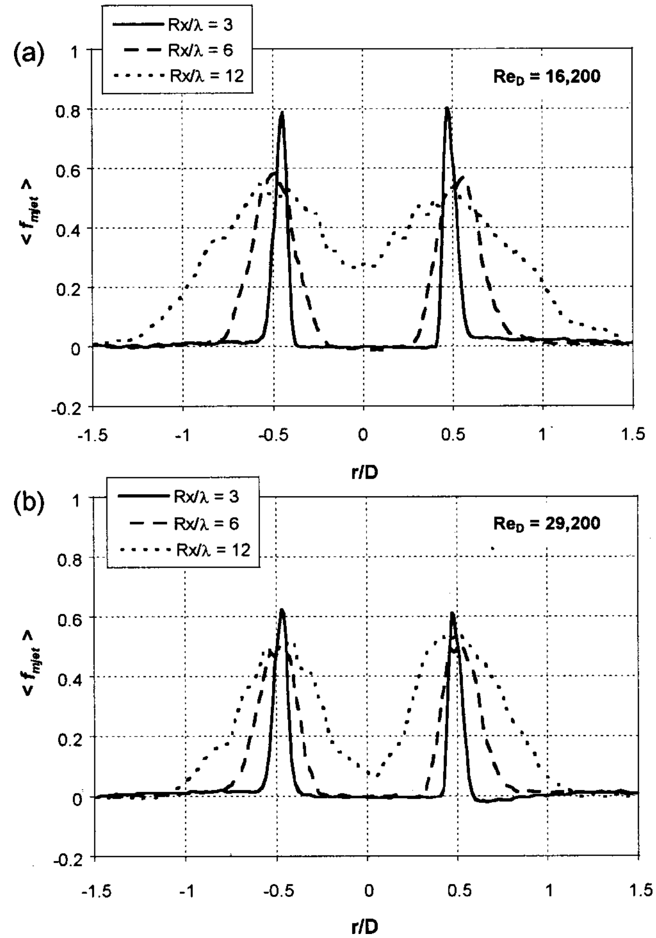

FIG. 8. Ensemble-averaged mixed jet fluid fraction, $\langle f_{\mathrm{mjet}} \rangle$, for (a) $\mathrm{Re}_D = 16\,200$ and (b) $\mathrm{Re}_D = 29\,200$.

cused on defining the location of the mixing transition more precisely, and on determining how the instantaneous shear-layer structure discussed in the previous section affects the mixed-jet fluid fraction statistics.

The ensemble-averaged mixed-jet fluid fraction, $\langle f_{\mathrm{mjet}} \rangle$, for $\mathrm{Re}_D = 16\,200$, 22 700, and 29 200 was calculated from 75, 75, and 50 instantaneous images, respectively, in order to determine the effects of the mixing transition on the statistical composition of the shear layer. Three cross-sections of $\langle f_{\mathrm{mjet}} \rangle$ are shown in Fig. 8 for $\mathrm{Re}_D = 16\,200$ and 29 200. The symmetry about the jet centerline is excellent, and indicates that the number of images used in the ensemble is adequate for statistical analysis. Symmetry also allows the use of both sides of the shear layer for the calculation of all subsequent statistical quantities. The axial locations of the cross-sections of $\langle f_{\mathrm{mjet}} \rangle$ in Fig. 8 represent various stages of mixing layer evolution, and will be referred to frequently in the following discussion. These locations correspond to regions near the initial vortex roll-up ($Rx/\lambda \approx 3$), first vortex pairing ($Rx/\lambda \approx 6$), and second vortex pairing ($Rx/\lambda \approx 12$). Note that the shear layer widths for $\mathrm{Re}_D = 16\,200$ and 29 200 are similar at $Rx/\lambda = 3$ and 6, but the shear layer width at $Rx/\lambda = 12$ is narrower for the higher Reynolds number.

The mixed jet fluid volume fraction, V_{mj}/V, accounts for radial weighting effects of $\langle f_{\mathrm{mjet}} \rangle$ in axisymmetric shear layers [see Eq. (5)], and can be used to reveal changes in the behavior of $\langle f_{\mathrm{mjet}} \rangle$ in the axial direction. Plots of V_{mj}/V, are shown in Fig. 9 for $\mathrm{Re}_D = 16\,200$, 22 700, and 29 200, and for both x/D and Rx/λ axial scaling. The plot of V_{mj}/V for

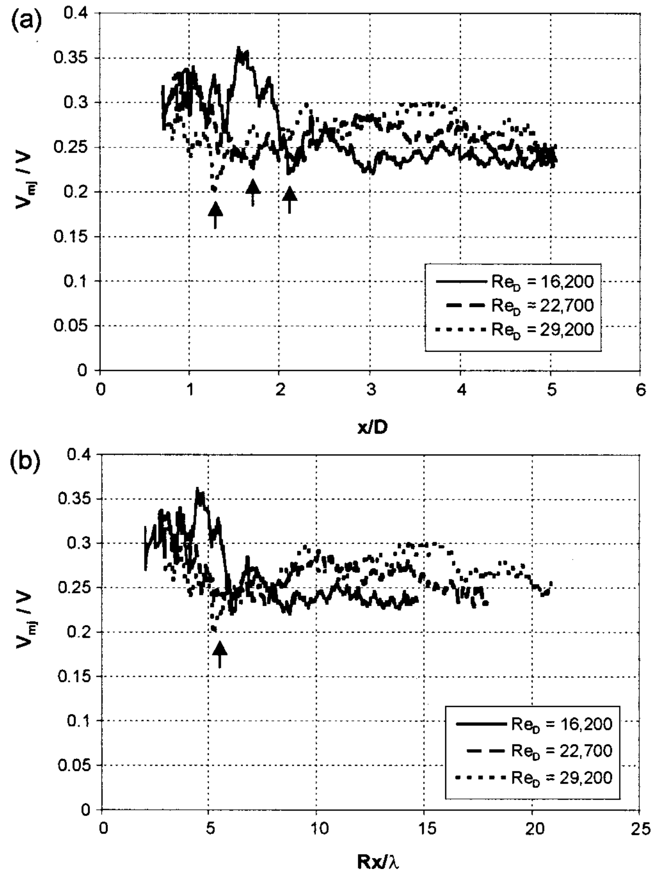

FIG. 9. Mixed jet fluid volume fraction plotted along (a) the axial coordinate, x/D, and (b) the pairing parameter, Rx/λ.

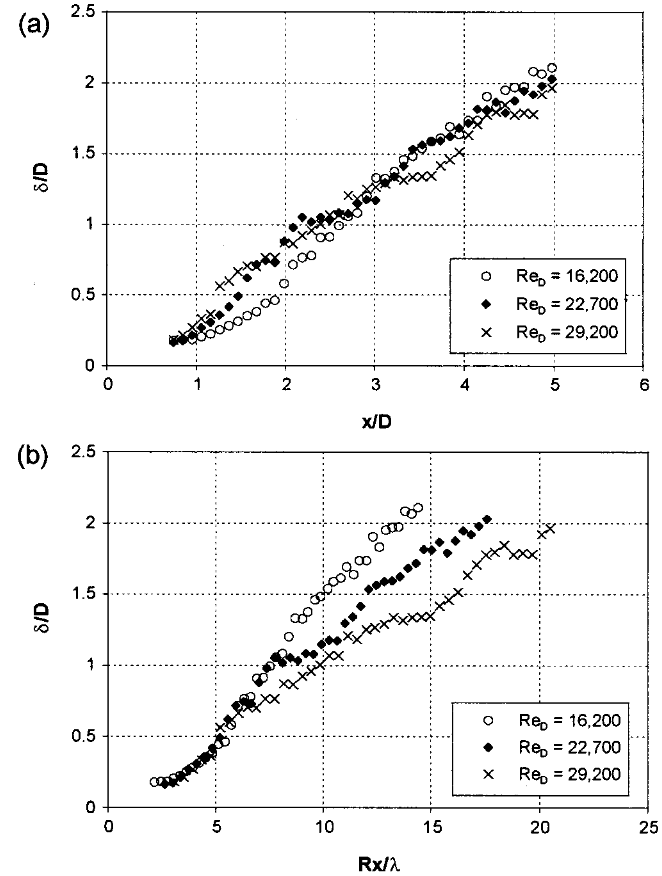

FIG. 10. Mixing layer width plotted along (a) the axial coordinate, x/D, and (b) the pairing parameter, Rx/λ.

$\mathrm{Re}_D=16\,200$ remains relatively constant at $V_{mj}/V \approx 0.3$ for a certain axial distance, drops suddenly at about $x/D \approx 2$, then remains nearly constant at $V_{mj}/V \approx 0.23$. Note that this sudden drop corresponds to the typical location of the first pairing for $\mathrm{Re}_D=16\,200$, and may be partially due to the co-flow fluid engulfment that occurs during pairing [see Fig. 3(a), third and fourth images, $x/D \approx 3$]. Since V_{mj}/V measures the average mixed jet fluid volume fraction rather than the average total mixed fluid volume fraction, co-flow fluid engulfment leads to a drop in V_{mj}/V. Koochesfahani and Dimotakis,[20] for example, found a similar drop in high-speed fluid concentration but an increase in total mixed fluid during the mixing transition. In addition to co-flow fluid engulfment, the drop in V_{mj}/V is consistent with the appearance of low f_{mjet} secondary structures on the co-flow boundary of the shear layer.

By comparison with these trends at $\mathrm{Re}_D=16\,200$, the profiles at $\mathrm{Re}_D=22\,700$ and $29\,200$ have shorter initial regions of constant V_{mj}/V, since vortex roll-up has already taken place prior to $x/D=1$, but a similar drop in V_{mj}/V is seen near the typical location of the first vortex pairing for $\mathrm{Re}_D=22\,700$ and $29\,200$. Thus, when V_{mj}/V is plotted in terms of Rx/λ in Fig. 10(b), the location of this drop nearly coincides for all Reynolds numbers at $5.4 < Rx/\lambda < 6$.

The growth of the $\pm 5\%$ $\langle f_{\mathrm{mjet}} \rangle$ shear layer width, δ/D, is plotted in Fig. 10 for $\mathrm{Re}_D=16\,200$ and $29\,200$ using both the x/D and Rx/λ axial scaling. The collapse of the pre-pairing profiles of δ/D vs Rx/λ in Fig. 10(b) is remarkable, and indicates that the pairing parameter provides the appropriate length scale in the region dominated by Kelvin–Helmholtz rollers ($Rx/\lambda < 6$). The divergence of the post-pairing profile of δ/D vs Rx/λ in Fig. 10(b) is also remarkable, in that it indicates that a fundamental shift in the nature of the mixing process has occurred ($Rx/\lambda > 6$). The nearly co-linear profiles of δ/D vs x/D in the post-pairing region of Fig. 10(a) suggest that the mixing process after the first pairing is, in fact, turbulent in nature. The x-dependence and co-linearity occur because $\delta \propto R(x-x_o)$ under turbulent conditions, where x_o is the virtual origin, and $R=(1-r)/(1+r)$ is nearly identical for all the Reynolds numbers in the current investigation (see Table I). The onset of turbulence after the first vortex pairing event agrees with the results of Huang and Ho,[7] who found that random fine eddies are first detected during the first pairing, and with Moser and Rogers,[8] who found that the breakdown to small-scales for transitional Reynolds numbers begins as streamwise vortices are engulfed into the first pairing structure.

It is somewhat surprising to find that the radial positions of the mixing layers for $\mathrm{Re}_D=16\,200$ and $29\,200$ collapse when scaled with Rx/λ, as shown in Fig. 11. The radial position of the shear layer, as defined here, simply tracks the radial position of the peak $\langle f_{\mathrm{mjet}} \rangle$ at each axial location. Figure 11 indicates that the shear layer moves slightly outward in the near-exit region. Near $Rx/\lambda=6$, the outward move-

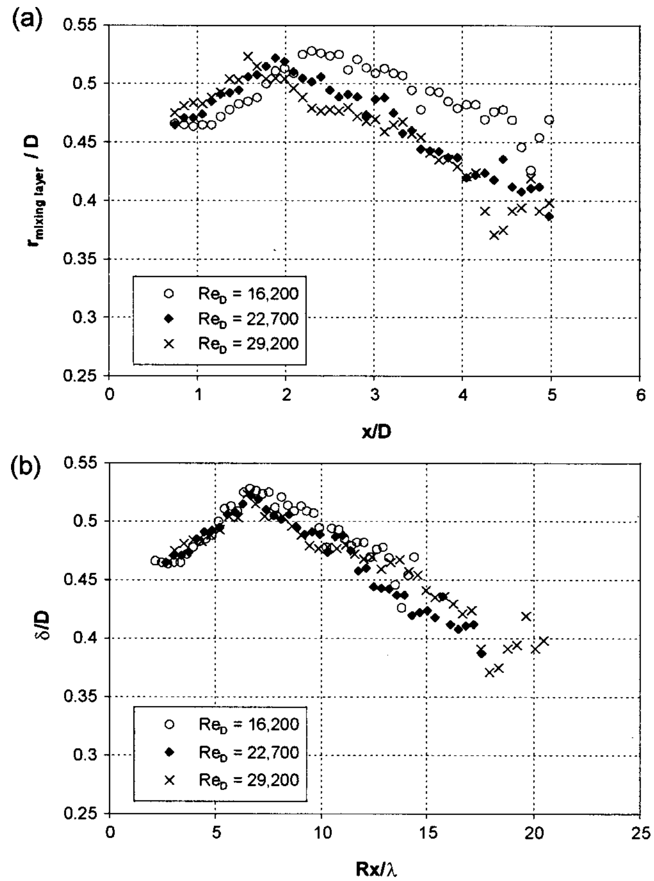

FIG. 11. Average radial position of the mixing layer plotted along (a) the axial coordinate, x/D, and (b) the pairing parameter, Rx/λ.

ment ends, and the shear layer begins to move inward.

The fact that the radial position of the shear layer in Fig. 11 does scale with Rx/λ may, in fact, reveal an important feature in the evolution of the mixing layer after the mixing transition. The instantaneous images discussed in the previous section were found to have a multi-layered structure. As shown in Figs. 6 and 7, the jet side of the shear layer is typically composed of large primary structures of high f_{mjet}, while the co-flow side is frequently composed of large structures of low f_{mjet}. The latter were also referred to as secondary structures with lower scalar dissipation outlines in Fig. 4. Since the radial position of the shear layer measures the position of the peak value of $\langle f_{\mathrm{mjet}}\rangle$, it will therefore be dependent on the inner or primary structures. As noted in the scalar dissipation maps of Fig. 4, braid regions appear to exist beyond the mixing transition, suggesting organized motion subject to a Kelvin–Helmholtz-type instability. These primary structures may, therefore, maintain their dependence on initial instabilities longer than the secondary structures. Indeed, braid regions have been found in self-similar turbulent mixing layers[19] and turbulent jets,[30] as well, and have been shown to be affected by upstream disturbances such as tripping[18] and forcing.[19]

The instantaneous images indicate, on the other hand, that the secondary structures are composed of fluid that has been ejected from the primary structures, perhaps during vortex pairing and other large-scale interactions. An example of this is shown in the rightmost regions of Rows *A* and *B* in Fig. 6(a), in which the remnant tail of a paired structure with $f_{\mathrm{mjet}}\approx 0.3$ seems "cut-off" from the main structure. Many examples of such fluid ejections are visible in the maps of f_{mjet} in Fig. 3. Hot-wire studies in a high-Reynolds number axisymmetric shear layer have shown that an azimuthal mode structure, composed of streamwise vortices, develops on the exterior of the shear layer that advects fluid into and out of the shear layer.[10] Because these streamwise vortices are found on the outside of the layer, they are more slowly convected downstream and can exist for many passages of the primary structures. Since δ/D in Fig. 10 measures the $\pm 5\%$ $\langle f_{\mathrm{mjet}}\rangle$ width of the shear layer, its axial growth will tend to be dependent on the growth of both the primary and such secondary structures.

D. Probability density functions

Probability density functions (PDFs) of the mixed-jet fluid fraction, as defined by Eq. (6), can be extremely valuable in detecting statistically relevant changes within the mixing layer. Unlike ensemble-averaged statistical quantities, which are subject to large-scale structure intermittency, PDF shapes show the likelihood of finding pure fluid (tagged as 0 or 1), indicate the range of f_{mjet} values found at a particular location (by a narrow or broad shape), and show the most likely or preferred f_{mjet} value at a particular location (from the peak in the profile). Note that because the resolution of the imaging system (51 μm in-plane, 250 μm out-of-plane) is greater than the smallest diffusion length scale (see Table I), values of f_{mjet} give the amount of molecularly mixed fluid averaged over a pixel. Since the relative resolution varied by less than a factor of two within the imaged region for all conditions (see Table I), PDFs of f_{mjet} from 2×2 binned images were compared with PDFs from non-binned images to verify that changes in PDF shape and character were attributable to changes in flowfield characteristics. Note that pixel averaging precludes the measurement of absolute PDF shapes.

Figure 12 plots the PDF of f_{mjet} along the axial coordinate for $\mathrm{Re}_D=16\,200$, 22 700, and 29 200 using 5% f_{mjet} concentration bins (measurement uncertainty), 250 μm spatial bins (limiting resolution), and Rx/λ scaling. In order to avoid bias errors due to shear layer growth and movement, the axial path traced in the PDFs of Fig. 12 corresponds to the radial location of the peak $\langle f_{\mathrm{mjet}}\rangle$ (see Fig. 11). The most notable aspect of the PDFs of Fig. 12 is that the mixing layer seems to be composed of two main axial regions, the first with a preferred f_{mjet} in the range of 0.75–0.8, and the second in the range of 0.55–0.6 (values determined from a top-view of PDFs plotted in Fig. 12). This drop in the value of the preferred f_{mjet} is consistent with the drop in V_{mj}/V shown previously in Fig. 9. Figure 12 also shows that between the two main axial regions, the PDFs become broader, meaning that a wider range of f_{mjet} values occurs in this region. This is certainly consistent with the convoluted structures and folding layers of high and low f_{mjet} seen in the intermediate regions of the instantaneous images.

The transition from one axial region to the next in Fig.

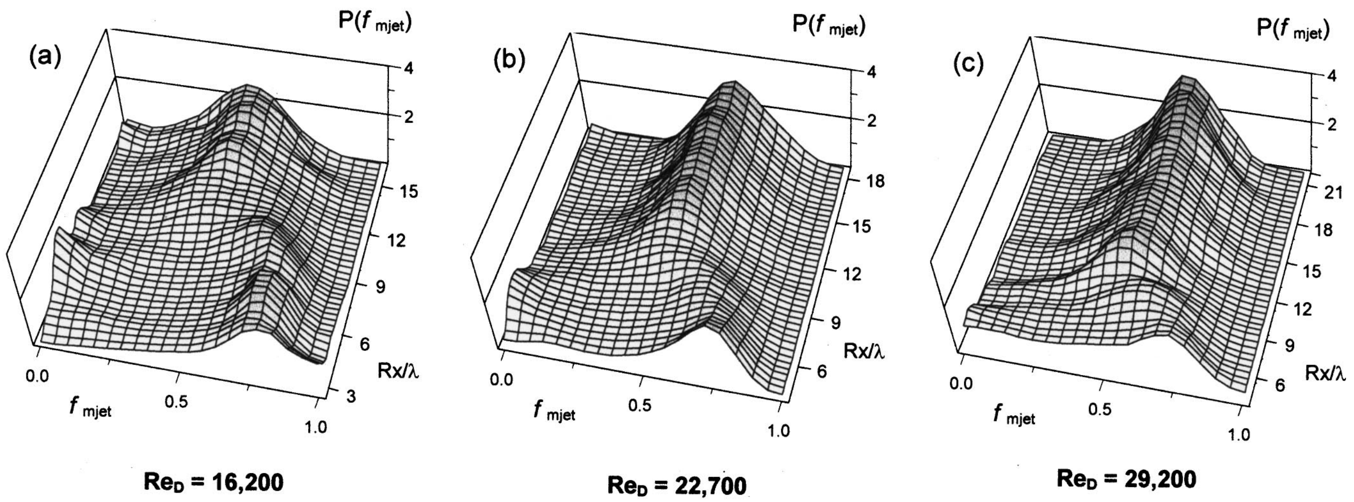

FIG. 12. Evolution of axial probability density functions of mixed jet fluid fraction along the shear layer plotted against the pairing parameter, Rx/λ, at (a) $\mathrm{Re}_D=16\,200$, (b) $\mathrm{Re}_D=22\,700$, and (c) $\mathrm{Re}_D=29\,200$. The PDFs were determined at a radial location corresponding to the peak value of $\langle f_{\mathrm{mjet}}\rangle$ at each axial location.

12 seems to begin after the first pairing ($Rx/\lambda>6$) for all three Reynolds numbers, which agrees with the small-scale transition detected in the ensemble-averaged statistics. The PDFs of Fig. 12, however, indicate that the transition takes place over a region that ranges from the location of the first pairing and is complete by the second pairing ($Rx/\lambda\approx12$).

Designating the location of the end of the mixing transition, however, depends on the criterion used to define this transition. Studies in planar shear layers indicate, for example, that the scalar field is not fully developed until about $Rx/\lambda\approx22$[18] rather than at $Rx/\lambda\approx12$ as indicated by the axial PDFs of Fig. 12. This conclusion in planar shear layers was obtained by studying radial PDFs, however, which may evolve differently than axial PDFs. Radial PDFs of f_{mjet} using 5% concentration bins and 250 μm spatial bins are shown in Fig. 13 for $\mathrm{Re}_D=16\,200$, 22 700, and 29 200, and for $Rx/\lambda=6$, 9, 12, and 15. Note, first of all, that the PDFs for all three Reynolds numbers have similar structures at all common values of Rx/λ. At $Rx/\lambda=6$, for example, the PDFs remain at a constant preferred f_{mjet} radially across the entire mixing layer. This ''stationary'' PDF is indicative of the large-scale roller structures that entrain pure fluid across the entire width of the mixing layer, and can also be expected in the post-pairing structures that are in the process of homogenizing those pure fluid layers. Note the significant intermittency during this stage is evident from the large values of $P(f_{\mathrm{mjet}})$ at $f_{\mathrm{mjet}}=0$ within the shear layer ($0.4<r/D<0.7$).

At $Rx/\lambda=9$, which is in between initiation and completion of the mixing transition, the radial PDFs are stationary on the jet side (towards $r/D=0$), but the occurrence of the secondary structures noted in Fig. 4 becomes visible from the low values of f_{mjet} towards the co-flow side. This PDF behavior on the co-flow side is often referred to as marching, since the peak f_{mjet} value in the PDFs translates as one moves in the radial direction. The existence of stationary PDFs on the jet side and marching PDFs on the co-flow side has been referred to as ''hybrid'' by King *et al.*,[13] and as ''dual'' by Karasso and Mungal.[18] The radial PDFs of Fig. 13 are consistent with the location of the PDF shift cited by King *et al.*[13] as occurring by $Rx/\lambda\approx12-14$. Some evidence of the PDF shift seems to appear as early as $Rx/\lambda=6$ in Figs. 13(a) and 13(c) at $r/D\approx0.75$, however and, along with the axial PDFs of Fig. 12, seems to indicate that the mixing transition takes place in the region between $Rx/\lambda=6$ and 12. This agrees with the axial PDFs discussed above but differs from the ensemble-averaged results, in which the transition process seems to be very short and take place near $Rx/\lambda=6$. The prominence of the marching behavior on the co-flow side increases with Rx/λ until $Rx/\lambda=15$, as shown in Fig. 13, and for PDFs beyond $Rx/\lambda=15$ (not shown in Fig. 13). The radial PDFs indicate, therefore, that the preferred f_{mjet} in the shear layer is still changing in the radial direction, albeit slowly, well beyond the second pairing at $Rx/\lambda\approx12$. This is not surprising given the results of Karasso and Mungal,[18] who found a similar evolution from stationary to marching PDFs beyond the mixing transition. In defining the location of the transition, however, it seems appropriate to identify the region in which the change in mixing behavior is ''sudden'' and ''dramatic,'' and not on whether the asymptotic PDF behavior has been attained. Thus, Figs. 12 and 13 indicate that the most dramatic changes in PDF behavior occur between the first and second pairing at $Rx/\lambda=6$ and 12, respectively. This agrees with the mixing transition reported by Breidenthal[17] between $Rx/\lambda=8-12$.

In interpreting the underlying shear layer structure responsible for the marching behavior on the co-flow side, it is important to reconcile the PDFs of Fig. 13 with the instantaneous structures shown in Figs. 3–7. The stationary PDFs on the jet side certainly support the existence of homogeneous primary structures in this region. Note as well that there is some degree of intermittency remaining on the jet side at high Rx/λ that is indicative of the passage of braid regions, as well as some intrusion of pure fluid within the primary structures on the jet side of the mixing layer.

On the other hand, the seemingly homogeneous nature

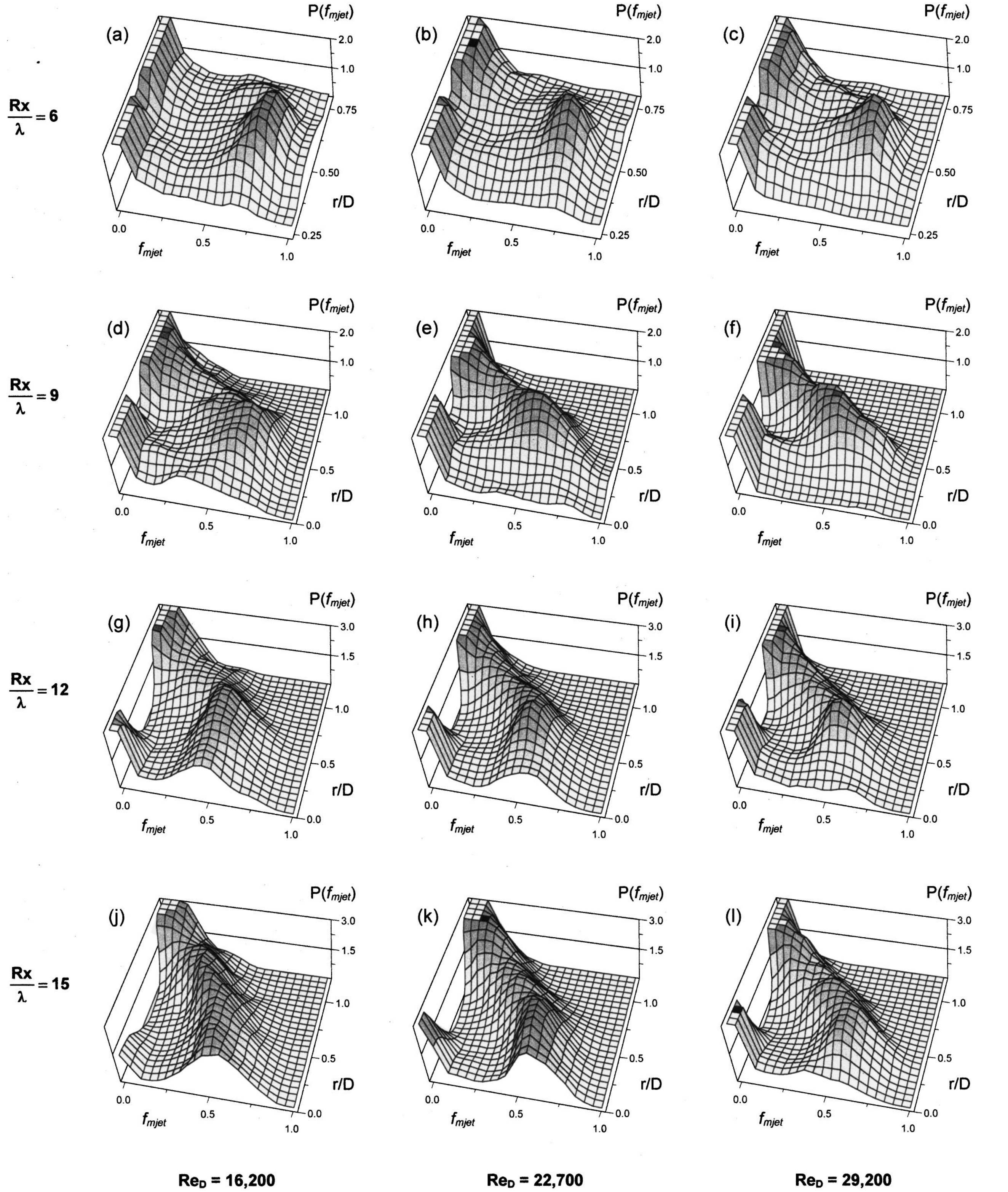

FIG. 13. Evolution of radial probability density functions of mixed jet fluid fraction, f_{mjet}, for $\mathrm{Re}_D = 16\,200$, 22 700, and 29 200 at axial locations of (a)–(c) $Rx/\lambda = 6$, (d)–(f) $Rx/\lambda = 9$, (g)–(i) $Rx/\lambda = 12$, and (j)–(l) $Rx/\lambda = 15$.

of the secondary structures, shown in Fig. 4 and manifested in the multi-level profiles of Figs. 6 and 7, seems to contradict the marching PDF behavior on the co-flow side. However, if the secondary structures have intermittent radial positions, the multi-level profiles in Figs. 6 and 7 (Rows *C* and *D*) will be smoothed and will result in marching rather than stationary statistics. In addition, PDFs that march to a preferred $f_{\mathrm{mjet}} = 0$ on the co-flow side of the mixing layer indicate that the secondary structures undergo small-scale gradient-like turbulent diffusion with the co-flow fluid.

King *et al.*[13] found hybrid radial PDF behavior similar to that shown in Fig. 13 at Reynolds numbers up to $\mathrm{Re}_D = 10\,000$, although with a significantly reduced radial extent of the jet-side stationary PDF region. This indicates that the primary structures on the jet side of the mixing layer maintain their pre-transition homogeneous composition for a significant downstream distance, but turbulent small-scale mixing with secondary structures decreases the radial extent of the homogeneous regions beyond the mixing transition. Pure fluid intrusions and continual homogenization on the jet side of the mixing layer, on the other hand, help maintain a small degree of stationary PDF behavior well beyond the mixing transition.

V. CONCLUSIONS

The location and nature of the mixing transition prior to the end of the jet potential core in initially laminar, high Reynolds number axisymmetric jets were studied using instantaneous images of molecularly mixed-jet fluid fraction. Maps of scalar dissipation were used to highlight the convoluted diffusion layers in the transitional large-scale structures, and the jet fluid mixing efficiency was used to determine the location and extent of subresolution stirring. Ensemble averages and probability density functions were used to measure changes in the mixing layer composition that are indicative of a transition to small-scale mixing. These changes include a 20%–25% drop in the mixed jet fluid volume fraction, a sudden change in the growth rate of the shear layer, and a 30%–35% drop in the preferred mixed-jet fluid fraction.

In addition to viewing the mixing transition on a qualitative basis, instantaneous images also helped in the physical interpretation of the statistical quantities. The instantaneous images revealed that the mixing transition initiates an internal cascade of scales within pairing vortices, and also initiates the ejection of mixed fluid of varying concentrations away from the shear layer toward the co-flow fluid stream. The composition downstream of the mixing transition, therefore, consists of primary structures that remain on the interface with the jet fluid stream and secondary structures on the exterior of the mixing layer. The primary structures maintain a mixed-jet fluid fraction at 75% of the pre-transition level of $f_{\mathrm{mjet}} = 0.8$, and seem to entrain pure jet fluid partially into the shear layer downstream of the mixing transition. The secondary structures have a typical mixed-jet fluid fraction at 25% of the pre-transition level. This results in a radial probability density function of mixed-jet fluid fraction beyond the mixing transition that is stationary near the jet core and marching towards the co-flow.

Ensemble averages and probability density functions were also used to determine statistically the location of the mixing transition. The mixing layer was found to undergo a dramatic transition to smaller scales and higher mixing at a downstream location determined by the initial instability wavelength and velocity ratio. The appropriate nondimensional axial scaling was thus confirmed to be the pairing parameter, Rx/λ. Ensemble-averaged statistics indicated that the location of the mixing transition begins near $Rx/\lambda = 6$, or shortly after the first vortex pairing, for all Reynolds number cases studied.

In addition, probability density functions of f_{mjet} in the axial direction indicated, from a shift in the preferred f_{mjet} value, that the mixing transition continues until the second pairing at about $Rx/\lambda = 12$ for all Reynolds numbers studied. This shift in the preferred f_{mjet} provides the strongest indication of the initiation and completion of the sudden and dramatic transition to small mixing scales. Radial probability density functions confirmed that the location of the mixing transition occurs between the first and second pairings at $Rx/\lambda = 6$ and 12, respectively. By comparison, previous investigations in planar shear layers predict that pairing occurs earlier with respect to Rx/λ,[7] but that the mixing transition occurs similarly from $Rx/\lambda = 8$–12.[17] Finally, in agreement with previous investigations,[13,16] an evolution in mixed-fluid PDFs from stationary to hybrid behavior is observed beyond the mixing transition.

ACKNOWLEDGMENTS

This work was supported by the National Science Foundation, Division of Chemical and Transport Systems, Grant No. CTS 94-23280, with Dr. R. E. A. Arndt and Dr. J. F. Foss as monitors.

[1] J. H. Konrad, "An experimental investigation of mixing in two-dimensional turbulent shear flows with applications to diffusion-limited chemical reactions," California Institute of Technology, Report No. CIT-8-PU, 1976.
[2] G. F. King, R. P. Lucht, and J. C. Dutton, "Quantitative dual-tracer planar laser-induced fluorescence measurements of molecular mixing," Opt. Lett. **22**, 633 (1997).
[3] G. F. King, R. P. Lucht, and J. C. Dutton, "Instantaneous dual-tracer PLIF measurements of molecular mixing in axisymmetric jets," AIAA Paper No. 97-0152, 35th AIAA Aerospace Sciences Meeting and Exhibit, Reno, NV, 1997.
[4] S. C. Crow and F. H. Champagne, "Orderly structure in jet turbulence," J. Fluid Mech. **48**, 547 (1971).
[5] C. D. Winant and F. K. Browand, "Vortex pairing: the mechanism of turbulent mixing-layer growth at moderate Reynolds number," J. Fluid Mech. **63**, 237 (1974).
[6] L. P. Bernal and A. Roshko, "Streamwise vortex structure in plane mixing layers," J. Fluid Mech. **170**, 499 (1986).
[7] L. S. Huang and C. M. Ho, "Small-scale transition in a plane mixing layer," J. Fluid Mech. **210**, 475 (1990).
[8] R. D. Moser and M. M. Rogers, "Mixing transition and the cascade to small scales in a plane mixing layer," Phys. Fluids A **3**, 1128 (1991).
[9] W. Schoppa, F. Hussain, and R. W. Metcalfe, "A new mechanism of small-scale transition in a plane mixing layer: core dynamics of spanwise vortices," J. Fluid Mech. **298**, 23 (1995).
[10] J. Citriniti, "Azimuthal mode interaction in an unforced high Reynolds-number axisymmetric shear layer," AIAA Paper No. 97-1810, 28th AIAA Fluid Dynamics Conference, Snowmass Village, CO, 1997.
[11] I. Danaila, J. Dusek, and F. Anselmet, "Coherent structures in a round, spatially evolving, unforced, homogeneous jet at low Reynolds numbers," Phys. Fluids **9**, 3323 (1997).
[12] N. T. Clemens and P. H. Paul, "Scalar measurements in compressible axisymmetric mixing layers," Phys. Fluids **7**, 1071 (1995).
[13] G. F. King, J. C. Dutton, and R. P. Lucht, "Instantaneous, quantitative measurements of molecular mixing in the axisymmetric jet near field," Phys. Fluids **11**, 403 (1999).
[14] A. K. M. F. Hussain and K. B. M. Q. Zaman, "Vortex pairing in a circular jet under controlled excitation. Part 2. Coherent structure dynamics," J. Fluid Mech. **101**, 493 (1980).
[15] T. R. Meyer, J. C. Dutton, and R. P. Lucht, "Vortex interaction and mixing

in a driven gaseous axisymmetric jet,'' Phys. Fluids **11**, 3401 (1999).
[16] C. M. Ho and P. Huerre, ''Perturbed free shear layers,'' Annu. Rev. Fluid Mech. **16**, 365 (1984).
[17] R. Breidenthal, ''Structure in turbulent mixing layers and wakes using a chemical reaction,'' J. Fluid Mech. **109**, 1 (1981).
[18] P. S. Karasso and M. G. Mungal, ''Scalar mixing and reaction in plane liquid shear layers,'' J. Fluid Mech. **323**, 23 (1997).
[19] M. M. Rogers and R. D. Moser, ''Direct simulation of a self-similar turbulent mixing layer,'' Phys. Fluids **6**, 903 (1994).
[20] N. T. Clemens and M. G. Mungal, ''Large-scale structure and entrainment in the supersonic mixing layer,'' J. Fluid Mech. **284**, 171 (1995).
[21] M. M. Koochesfahani and P. E. Dimotakis, ''Mixing and chemical reactions in a turbulent liquid mixing layer,'' J. Fluid Mech. **170**, 83 (1986).
[22] M. G. Mungal and P. E. Dimotakis, ''Mixing and combustion with low heat release in a turbulent shear layer,'' J. Fluid Mech. **148**, 349 (1984).
[23] C. E. Frieler, Ph.D. thesis, California Institute of Technology, 1992.
[24] K. A. Buch and W. J. A. Dahm, ''Experimental study of the fine-scale structure of conserved scalar mixing in turbulent shear flows. Part 2. Sc ~ 1,'' J. Fluid Mech. **364**, 1 (1998).
[25] R. E. Drubka, P. Reisenthel, and H. M. Nagib, ''The dynamics of low initial disturbance turbulent jets,'' Phys. Fluids A **1**, 1723 (1989).
[26] A. Michalke, ''On spatially growing disturbances in an inviscid shear layer,'' J. Fluid Mech. **23**, 521 (1965).
[27] P. A. Monkewitz and P. Huerre, ''The influence of the velocity ratio on the spatial instability of mixing layers,'' Phys. Fluids **25**, 1137 (1982).
[28] E. Gutmark and C. M. Ho, ''Preferred modes and the spreading rates of jets,'' Phys. Fluids **26**, 2932 (1983).
[29] H. S. Hussain and F. Hussain, ''Experiments on subharmonic resonance in a shear layer,'' J. Fluid Mech. **304**, 343 (1995).
[30] W. J. A. Dahm and P. E. Dimotakis, ''Measurements of entrainment and mixing in turbulent jets,'' AIAA J. **25**, 1216 (1997).